Albumin Nanoparticles for the Delivery of a Novel Inhibitor of β-tubulin Polymerization

Alessandra Spada[1,2], Jaber Emami[3,4], Forough Sanaee[3], Maral Aminpour[1], Igor M. Paiva[3], Jack A. Tuszynski[1,2], Afsaneh Lavasanifar[3]

[1]Department of Oncology, Cross Cancer Institute, University of Alberta, Edmonton, Alberta, Canada; [2]DIMEAS, Politecnico di Torino, Turin, Italy; [3]Faculty of Pharmacy and Pharmaceutical Sciences, University of Alberta, Edmonton, Alberta, Canada; [4]School of Pharmacy and Pharmaceutical Sciences, Isfahan University of Medical Sciences, Isfahan, Iran.

Corresponding authors: Afsaneh Lavasanifar, Faculty of Pharmacy and Pharmaceutical Sciences, University of Alberta; Edmonton, Alberta, T6G 2R3, Canada; email: afsaneh@ualberta.ca; Jack A. Tuszynski, Department of Oncology, Cross Cancer Institute, University of Alberta, Edmonton, Alberta, T6G 1Z2, Canada; email: jackt@ualberta.ca

Received, April 30, 2021; Revised, June 25, 2021; Accepted, June 28, 2021; Published, July 3, 2021

ABSTRACT -- Purpose: The ultimate goal of this study is to develop a novel delivery system for a new potent cytotoxic compound, CCI-001, with anti-β tubulin activity, so that the drug can be effectively administered and at the same time its harmful side effects can be reduced. **Methods:** In the current study, CCI-001 was loaded into serum albumin (SA), using a modified desolvation method, generating CCI-001-SA nanoparticles. Both bovine and human SA were used for the encapsulation of this drug candidate. Optimum conditions for drug loading were achieved when already formed and crosslinked albumin nanoparticles were incubated overnight at 37°C with CCI-001 solutions. The CCI-001-loaded albumin nanoparticles were assessed for average particle diameter and polydispersity, zeta potential, drug loading, *in vitro* release, morphology and cell toxicity against SW620 and HCT116 colorectal cancer cells. **Results:** The spherical nanoparticles obtained were negatively charged (~ -30 mV) and had an average diameter of ~ 130 nm, with a narrow size distribution. The *in vitro* release of CCI-001 from the albumin nanoparticles showed a sustained release pattern over 24 hours without any initial burst release, compared to the fast release of the free drug under experimental conditions. No difference between the SA from the two species in terms of CCI-001 loading was observed. However, a significant difference was observed between the release profiles of CCI-001 from drug-loaded HSA and drug-loaded BSA nanoparticles with HSA nanoparticles showing slower drug release (mean release time, MRT, values of 5.14 ± 0.33 h and 6.88 ± 0.15 h for BSA-NPs and HSA-NPs, respectively, $P < 0.01$). Cellular toxicity studies showed higher cytotoxicity for CCI-001-SA compared to the free drug (IC_{50}s of 0.62 ± 0.31 nM *vs* 2.06 ± 0.29 nM in SW620 cells and 0.9 ± 0.1 nM *vs* 4.2 ± 0.2 nM in HCT116 cells, for CCI-001-HSA NPs and free drug, respectively). Therefore, despite the low drug content level in the HSA nanoparticles of CCI-001, the formulation provides relevant concentrations for further *in vivo* studies in animal models due to high drug potency. **Conclusions:** The data support the potential use of albumin as a nanocarrier for CCI-001 in biological systems.

INTRODUCTION

Cancer is the second leading cause of death globally, exceeded only by cardiovascular diseases. In 2018, cancer was responsible for 9.6 million deaths worldwide (1). Conventional therapeutic options consist of surgery, radiotherapy, chemotherapy, immunotherapy and targeted therapy. One of the major limitations of conventional chemotherapy in cancer treatment is the wide range of side effects caused by anti-cancer drugs, which is attributed to their non-selective distribution and/or action on both cancer and normal dividing cells (2,3). The drawbacks of anti-cancer compounds led to the development of new and innovative formulations and drug delivery systems, aimed at increasing the solubility, permeability, biological half-life and/or reducing the non-specific distribution of anticancer agents, leading to an improvement in their therapeutic efficiency (4). In fact, the use of nanocarrier systems as an alternative platform to the conventional drug solubilization approaches which use a high concentration of toxic surfactants and/or co-solvents, can lead to the safer and more efficient clinical use of anticancer agents. Nanoparticles can augment drug levels at the site of action via passive and/or active targeting processes and reduce non-specific drug distribution to healthy tissues minimizing drug adverse effects (5). Colchicine, a major alkaloid isolated from the seeds and bulbs of *Colchicum autumnale* and

Gloriosa superba, has exhibited a wide range of therapeutic effects since its discovery by the French chemists P. S. Pelletier and J. B. Caventou in 1820 (6). Although it has been utilized as a therapeutic agent for years, its mechanism of action remained unknown until 1968, when tubulin was recognized as its main target (7). More recent studies (8,9) investigated its antiproliferative and antimitotic effect. Microtubules, composed of α-tubulin and β-tubulin, play vital roles in determining cell shape and cell movement. They are responsible for the internal transportation of organelles and the separation of chromosomes during cell mitosis. Colchicine is proven to suppress microtubule dynamics, therefore blocking the mitosis. The formation of a colchicine-tubulin complex, which leads to a conformational inflexibility of tubulin and prevents microtubule polymerization, has been recognized as the main mechanism of action for colchicine. The consequence is the alteration of the dynamic instability (10), a process of continuous turnover of tubulin in microtubules, which is mainly responsible for the vital role played by microtubules in cellular mitosis (11). A disrupted microtubule dynamic leads to mitotic arrest and cell death by apoptosis (12). For this reason, colchicine has also been explored in the treatment of cancer. The proliferation of cancer cells was proven to be more effectively inhibited by colchicine than that of healthy cells (13), since the former undergo mitosis at higher rates. Furthermore, in the 1930s, colchicine was found to have damaging effects on tumor vasculature (14), causing haemorrhage and extensive necrosis in both animal and human tumours. In particular, colchicine has been demonstrated to possess both anti-angiogenic and vasculature-disrupting effects. In 2009 colchicine was FDA-approved as a stand-alone drug for the treatment of Mediterranean fever and acute flares of gout, a common type of arthritis that causes intense pain, swelling, and stiffness in joints (15).

CCI-001 (Figure 1), a colchicine derivative, is a novel β-tubulin polymerization inhibitor, developed at the University of Alberta in order to increase its affinity for β-III tubulin and therapeutic index (16) since the application of colchicine was limited by its high toxicity profile (17,18,19). The β-III tubulin is a tubulin isotype overexpressed by the majority of tumors (20,21). In effect, the CCI-001 has shown enhanced potency, especially in taxane-resistant tumours, when compared to conventional chemotherapeutics and colchicine, showing IC_{50} values in the nM range (22,23,24). However, the extremely poor water solubility of CCI-001 (< 7 µg/mL at pH 7.4, logP of 2.58) makes the use and *in vivo* administration of this compound as a therapeutic agent challenging. Poorly water-soluble chemotherapeutic agents like paclitaxel (Taxol®) or docetaxel (Taxotere®) are generally solubilized in water containing high concentrations of surfactants and/or co-solvents, which exhibit serious adverse effects upon systemic administration. Therefore, efficient and surfactant-free alternative formulations such as lipid-, polymer- and albumin-based nanocarrier systems have widely been investigated for encapsulation and delivery of drugs with very low water solubility. In addition to overcoming low aqueous solubility, these nanosized carriers also provide many other advantages including enhanced tumour uptake, reduced systemic adverse effects, and improved therapeutic index (25). CCI-001 has recently entered phase I clinical trials in patients with recurrent and/or metastatic solid tumors. A suitable nano-formulation of this novel anticancer agent is expected to enhance its therapeutic index in cancer patients (26).

In this manuscript, encapsulation of CCI-001 in albumin-based nanoparticles which can actively target tumor tissues via gp60 receptor is described.

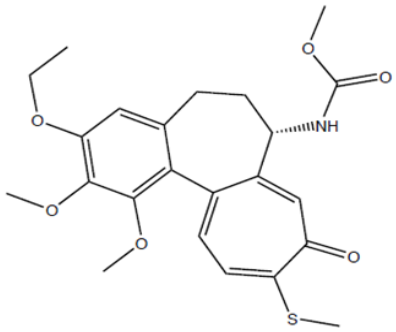

Figure 1. Chemical structure of CCI-001.

Albumin, one of the most abundant proteins in plasma, has been increasingly investigated as a carrier in nanomedicine, due to its unique features (27). Its biocompatibility, biodegradability, non-immunogenicity, non-toxicity and safety in clinical applications make the protein an appealing candidate in drug delivery. Besides, the chemical structure of the protein allows the interaction with both hydrophilic and hydrophobic compounds (28,29). The active recognition by the gp60 receptor (a 60 kDa glycoprotein) and SPARC (secreted protein, acidic and rich in cysteine), overexpressed in diseased tissues and cells, enhances the intratumoral accumulation of albumin nanoparticles, without the addition of specific

ligands to the nanocarrier (30). This accumulation of albumin in diseased tissues, such as that of solid tumours, provides a rationale for the development of albumin-based formulations, aimed at actively targeting the tumours. As the first FDA-approved (in 2005) albumin-based drug delivery system, Abraxane® (nab-paclitaxel, ABI-007) was developed to enhance the activity and reduce the side effects linked to the traditional solvent-based paclitaxel formulations (31,32).

Therefore, the objective of this study was to develop and evaluate albumin nanoparticles for the delivery of CCI-001. For this purpose, different albumin-based nanoparticle fabrication techniques including nab-technology, desolvation and modified desolvation were explored. Bovine serum albumin was used during the formulation optimization process. Once the formulation was optimized, the technique was repeated for the human serum albumin formulation of CCI-001, to assess any potential difference between the albumin from the two different species. The characteristics of obtained formulations such as size, zeta potential, morphology, encapsulation efficiency and *in vitro* release were analysed. Finally, the cytotoxic activity of the drug delivery system was tested on two colorectal cancer cell lines, HCT116 and SW620.

MATERIALS AND METHODS

Materials

CCI-001 ($C_{23}H_{27}NO_6S$) was provided by the Department of Oncology, University of Alberta, Edmonton, Canada. HSA (human serum albumin, lyophilized powder >96%, agarose gel electrophoresis) was obtained from Sigma Aldrich (Canada). BSA (bovine serum albumin, lyophilized powder) was purchased from Tocris Bioscience. Glutaraldehyde ($OHC(CH_2)_3CHO$, grade II, 25% in H_2O), also known as pentanedial, glutaral and 1,5-pentanedial, was provided by Sigma Aldrich (Canada). Sodium hydroxide (NaOH), was obtained from Sigma Aldrich (Canada). All the other chemicals used in this study were analytical or high-performance liquid chromatography (HPLC) grade. HCT116 and SW620, colorectal cancer cell lines, were obtained as a generous gift from the laboratory of Dr. Michael Weinfeld, Katz Group Centre, University of Alberta, Edmonton (Canada). The medium used for supporting the growth and development of the SW620 was the DMEM + F12 (Dulbecco's Modified Eagle Medium, provided by Thermo Fisher Scientific), enriched with 10% fetal bovine serum and 1% antibiotic penicillin-streptomycin. The medium used for the culture of HCT116 was the DMEM media (provided by Thermo Fisher Scientific), enriched with 10% fetal bovine serum and 1% penicillin-streptomycin.

Methods

Preparation of CCI-001-loaded albumin nanoparticles using different methods

Emulsification followed by sonication or high-pressure homogenization

In the present study, BSA nanoparticles were produced first using a method inspired by nab-technology (33,34), adopting two experimental techniques including sonication and high-pressure homogenization, which are two high (mechanical)-energy emulsification methods (35,36). Briefly, BSA was dissolved in double-distilled water (1% w/v, 25 mL) and stirred on a magnetic stirrer (Corning PC 353 Stirrer). A drug solution prepared in a mixture of chloroform and ethanol at a ratio of 9:1 (500 µL) was then added dropwise to the previously obtained BSA solution and stirred on a magnetic stirrer at 500 rpm for 30 min. The resulting dispersion was then sonicated (Sonicator® XL Ultrasonic Liquid Processor, Heat Systems) to produce a very fine emulsion and obtain nanoparticles. The developed formulation was then transferred to a rotary evaporator (Buch Rotavapor® and Buchi 461 WaterBath) operated for 30 minutes, and the organic solvent was removed at 40°C at reduced pressure. The system was then centrifuged (Sorvall Legend Micro 21 R Microcentrifuge, Thermo Scientific) at 5000 rpm for 5 minutes, to separate the non-loaded drug and precipitate the micro/macro particles from the nanoparticles. The particle size was measured in the upper phase. Different energies and powers of the sonicator were also used. The effect of the usage of a hand homogenizer (Grainger PRO250 Hand-Held Homogenizer) instead of a magnetic stirrer for mixing the water and the oil phases prior to sonication was also investigated. In some studies, a high-pressure homogenizer (Nano DeBEE Laboratory Homogenizer) was used in place of sonication (37,38). This time, the mixture of BSA and drug solution was transferred to a high-speed homogenizer (around 10,000 rpm), to obtain a crude emulsion. Then, the pre-mixed emulsion was transferred to a high-pressure homogenizer (at 20000 psi, for 6 cycles) to form the nanoparticles. After that, the organic solvents were evaporated at 40°C for 30 minutes in a rotary evaporator. The resultant dispersion was then centrifuged at 5000 rpm for 5 min.

Desolvation method

The second technique adopted to prepare nanoparticles was desolvation (39,40). Briefly, BSA was dissolved in double-distilled water (2% w/v, 2.5 mL) and stirred on the magnetic stirrer, adjusting the pH using 0.1 M NaOH. A drug solution, prepared by dissolving the drug (2.5 mg, 5 mg, 12.5 mg) in 8 mL of desolvating agent ethanol or acetone, was added dropwise to the BSA solution at 1 mL/min. After 30 minutes, a glutaraldehyde 8% solution (1.17 µL/mg albumin) was added to the system for crosslinking the nanoparticles and left overnight while stirring. The day after, the system was centrifuged at 14000 rpm for 20 minutes and the precipitate was collected and washed three times to remove the unreacted glutaraldehyde. At the end, the nanoparticle pellets were collected. Blank nanoparticles were prepared in the same manner without drug. This process was repeated at different pHs, drug to albumin ratios, using different desolvating agents as summarized in Table 1.

Table 1. BSA nanoparticle formulations of CCI-001 prepared with desolvation method.

Formulation	Desolvating agent	pH	Drug/BSA ratio
Blank*	Ethanol	8	-
D1	Ethanol	8	1/4
D2	Ethanol	8	1/10
D3	Acetone	8	1/10
D4	Ethanol	8	1/20
D5	Ethanol	5.5	1/10

*Blank nanoparticles were prepared without drug.

Modified desolvation method

The desolvation method was then modified to improve the formulation characteristics (41). BSA (10 mg, 15 mg, 25 mg, 50 mg) or HSA (10 mg) was dissolved in 2 mL double-distilled water and stirred on the magnetic stirrer, adjusting the pH to 8 using 0.1 M NaOH. After 30 minutes, 8 mL ethanol as the desolvating agent was added dropwise to the BSA (or HSA) solution at 1 mL/min. After that, the glutaraldehyde 8% solution (1.17 µL/mg albumin) was added to the system and stirred overnight. The day after, the formulation was centrifuged at 14500 rpm for 30 minutes and washed three times to remove the unreacted glutaraldehyde. The albumin nanoparticles were then collected. After that, a drug solution, obtained by dissolving 1 mg drug in specific ratios of ethanol and water (1/4), was added to the previously obtained albumin nanoparticles at different ratios of drug to albumin. The formulations were placed in the water bath sonicator (Cole Parmer 8852 Ultrasonic Cleaner) for 30 minutes and then incubated overnight in a water bath (VwR Shaking Water Bath) shaking at 75 rpm, 37°C. The day after, the system was centrifuged again at 14500 rpm for 30 minutes, in order to collect the final drug-loaded albumin nanoparticles. The ratio of water and ethanol in the drug solution was first optimized and the amount of BSA was modulated to obtain the best drug loading. Blank nanoparticles were prepared in the same manner without the drug. Table 2 shows the different formulations prepared based on the modified desolvation method.

Table 2. BSA and HSA nanoparticle formulations of CCI-001 prepared with a modified desolvation method.

Formulation	Type of albumin	Drug/Albumin (mg/mg)	EtOH/H_2O in drug solution (mL/mL)	Volume of NaOH (µL) **	pH
Blank*	BSA	1/10	-	25	8
MD1	BSA	1/10	1/4	25	8
MD2	BSA	1/15	1/4	25	8
MD3	BSA	1/25	1/4	25	8
MD4	BSA	1/50	1/4	25	8
MD5	BSA	1/50	1/4	Not added	7
Blank*	HSA	1/10	1/4	50	9
MD6	HSA	1/10	1/4	25	8
MD7	HSA	1/10	1/4	50	9

*Blank nanoparticles were prepared without drug; **(0.1 M)

Characterization of CCI-001-loaded albumin nanoparticles

Size and zeta potential. The hydrodynamic diameter, polydispersity index (PDI) and zeta potential of BSA nanoparticles, HSA nanoparticles, CCI-001-BSA nanoparticles and CCI-001-HSA nanoparticles were determined by dynamic light scattering (DLS) using Zeta-Sizer Nano (Malvern Instruments Ltd, Malvern, UK). The nanoparticles were dispersed in distilled water at 25°C and diluted 1:100. For the measurement of the size, 0.5 mL of sample were analyzed, using low volume disposable cuvettes. For the measurement of the zeta potential, 0.8 mL of sample was analyzed, using the zeta dip cell with a quartz cuvette. Any air bubbles present in the sample were removed before starting the zeta potential evaluation.

Nanoparticles morphology. The morphologies of CCI-001-BSA nanoparticles and CCI-001-HSA nanoparticles were evaluated using a scanning electron microscope (Field Emission Scanning Electron Microscope, Zeiss, GeminiSEM). Nanoparticle dispersion (0.1 mL, 1:100 dilution) was placed on a glass substrate and allowed to dry overnight. After drying, the nanoparticles were placed on metal support and coated with gold (Denton Sputtering System), to render them electrically conductive and examined under the microscope. Electron microscopy was performed using an accelerating voltage of 5 kV and a working distance of 5 mm. Pictures were taken at 45,000 and 16,000-fold magnification using secondary electron detection mode.

Drug entrapment efficiency. After centrifugation, the albumin-drug nanoparticles were re-dispersed first in 100 µL water and 1 mL ethanol was added. After that, the system was vortexed, transferred to the water bath sonicator for 1 hour and then centrifuged at 14,500 rpm for 30 minutes, in order to collect the drug in the upper phase. An HPLC method (described below) was used to determine the amount of loaded CCI-001 into BSA and HSA nanoparticles. The drug encapsulation efficiency (EE%) was defined as the percentage of loaded CCI-001 compared to the initial amount of drug supplied. Loading capacity (LC%) was calculated as the amount of loaded CCI-001 divided by the albumin weight.

$$EE\ (\%) = \frac{Amount\ of\ drug\ in\ nanoparticles}{Amount\ of\ drug\ supplied} * 100$$

$$LC\ (\%) = \frac{Amount\ of\ drug\ in\ nanoparticles}{Total\ weight\ of\ albumin\ and\ drug} * 100$$

In vitro drug release studies. The *in vitro* release of CCI-001 from the albumin nanoparticles was evaluated using the equilibrium dialysis method, in PBS (pH 7.4). Furthermore, as a control, the release of free CCI-001 from an ethanol solution was also investigated. Both freshly prepared and the lyophilized nanoparticles were re-dispersed in 2.5 mL water and vortexed. The free CCI-001 and CCI-001-albumin nanoparticles, with the same drug content as the free drug, calculated by taking into consideration the drug entrapment efficiency of the nanoparticle formulation, were transferred into a dialysis bag (Spectrapor, MW cut-off 3500 Da) and the system was placed into 450 mL of dissolution medium (PBS) while shaking at 50 rpm, 37°C. The dialysis bag was sealed at both ends. At selected time points, 0.1 mL of sample was removed from the inside of the dialysis bag and replaced with 0.1 mL double distilled water (or, in the case of the free drug, with the solvents used in the formulation, in the same ratios). After having collected the 0.1 mL samples, 0.2 mL of ethanol was added, vortexed and placed in the water bath sonicator for around 1 hour. After that, the samples were centrifuged for 30 minutes at 14,500 rpm, in order to extract the drug. The upper phases were analysed by HPLC for determining the amount of CCI-001 present. The remaining concentration obtained at t_i was subtracted from the initial concentration of CCI-001 at t_0 in the dialysis bag and used to plot the cumulative drug released (%) versus time. The extraction procedure and the release studies were repeated at least three times for each formulation, and average and standard deviation were calculated. The release profiles were compared using mean release time (MRT). Based on the release profiles, MRT was calculated using the following equation:

$$MRT = \frac{\sum_{i=1}^{n} t_{mid}\,\Delta M_i}{\sum_{i=1}^{n} \Delta M_i}$$

where, i is the sampling number, n is the last sampling number, t_{mid} is the time at the midpoint between t_i and t_{i-1} (calculated as $(t_i + t_{i-1})/2$) and ΔM_i is the additional amount of drug released between t_i and t_{i-1}.

HPLC analysis of CCI-001

A Varian Prostar 210 HPLC system was used for the quantification of CCI-001 in the samples. The mobile phase was an isocratic mixture of water and acetonitrile (70:30), containing 0.1% trifluoroacetic acid, and the separation was obtained by a Microsorb-MV 5 μm C18-100 Å column (4.6 x 250 mm). The flow rate was set at 1 mL/min, at room temperature and the detection wavelength was 386 nm (Varian Inc., Palo Alto, CA, USA). The retention time of CCI-001 was 3.7 min. The assay was found linear over the examined range of 3.12-1000 μg/mL in the mobile phase, with a calibration curve of $y = 1.0451x – 1.6946$ and a correlation coefficient of 0.999. The concentration of CCI-001 in the samples was determined from the aforementioned regression equation. The lowest limit of quantification was found to be 6.25 μg/mL. The inter- and intra-day variations were less than 10% for all concentrations. No interfering peak was observed.

Stability of freeze-dried nanoparticles upon cryoprotection

The optimal batches obtained with the modified desolvation (MD1 and MD7 in Table 2) were freeze-dried (VirTis, SP Scientific), in order to improve their long-term stability (42). After obtaining the drug-loaded nanoparticles, the formulation was transferred to a -80°C freezer and stored overnight. The day after, the frozen formulations were placed in the freeze-dryer for at least 48 hours. By lyophilizing the formulation, a solid powder that can be easily reconstituted to the original dispersion following the addition of double distilled water was obtained. The nanoparticles were lyophilized both in the presence of trehalose (2.5% w/v) (43,44) as cryoprotectant and without it. Usually, the nanoparticles, previously dispersed in 8 mL of water, were lyophilized and the solid powder obtained was reconstituted in 2.5 mL of water. The differences in size and zeta potential between the two samples were evaluated.

Cell toxicity studies

The cytotoxicity of free CCI-001, CCI-001-HSA nanoparticles and carrier alone was tested using 3-(4, 5-Dimethyl-2-thiazolyl)-2, 5-diphenyl-2H-tetrazolium bromide (MTT) assay (45). On day 1, the cells were seeded on 96-well plates with media (100 μL/well) and they were incubated at 37°C for 24 hours. The cell density was 2×10^3 cells/well for the HCT116 cell line and 4×10^3 cells/well for the SW620 cells. After plating, the cells were left to adhere to the plate overnight. The day after, the treatment (free CCI-001, CCI-001-loaded HSA nanoparticles and HSA nanoparticles without drug) was added to the wells at different concentrations and incubated at 37°C for 48 or 72 hours. The MTT solution was prepared (5 mg/mL in distilled water, 20 μL/well), filtered and added to the cells after the incubation period with the treatments. The cells were then homogenized (Titer Plate Shaker, Thermo Scientific) and incubated at 37°C for 3-4 hours. After checking the effective presence of the crystals at the microscope (Leitz Diavert Inverted Tissue Culture Workhorse Microscope with Phase Contrast), the media was removed and 100 μL DMSO was added to each well and mixed thoroughly on the shaker, in order to dissolve the crystals. The plates were analysed and the cell viability was detected by measuring the optical absorbance at 570 nm (Synergy H1 Hybrid Multi-Mode Reader, Biotek). The mean absorbance of each treatment was determined and converted to the percentage of viable cells relative to the control. The IC_{50} of the specific treatment was calculated from the plot of the % of viable cells versus log CCI-001 concentration.

Statistical analysis

Data are expressed as mean ± standard deviation (SD) of three separate experiments. Comparison of statistical data was conducted by Students t-test for two groups and one-way ANOVA for multiple groups. The P-values of less than 0.05 were considered statistically significant in all cases. The null hypothesis used in the statistical analyses of the current study proposes that there were no differences between certain characteristics of the generated data such as comparison between hydrodynamic sizes, encapsulation efficiencies, drug releases, and cytotoxicities.

RESULTS

Characterization of CCI-001-loaded albumin nanoparticles prepared by emulsification methods

The characteristics of the nanoparticles prepared with the emulsification methods indicated that the formulations produced using a sonicator had bigger diameters than the ones obtained using a high-pressure homogenizer. The average hydrodynamic diameters for nanoparticles prepared using sonication were found to be in the range 350-500 nm with a multimodal size distribution, characterized bypolydispersity indices between 0.3 and 0.6, too high compared to the PDI values usually obtained after optimization of the albumin nanoparticle preparation, which are always < 0.3 (46). Moreover, the nanoparticles tended to

aggregate producing much bigger particles of about 800 nm over a short period of time. The formulations produced using high-pressure homogenization showed sizes below 200 nm (of around 170 nm), but still a broad size distribution (PDI 0.3). The zeta potential values were in the range between -8 and -20 mV for the formulations produced with sonication, and around -25 mV for those produced with high-pressure homogenization.

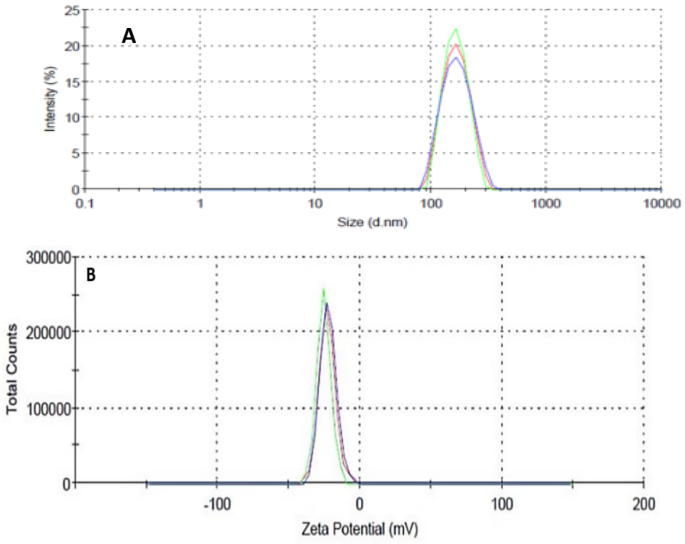

Figure 2. Representative particle size distribution (A) and zeta potential (B) diagram of CCI-001-loaded BSA nanoparticles prepared with emulsification method followed by high-pressure homogenization as measured by DLS. Each coloured line represents one replicate of the same formulation.

The entrapment efficiencies and consequently loading capacity of CCI-001 in BSA nanoparticles were always very low for both sonication and homogenization techniques (< 3% and 2%, respectively). Therefore, further investigations on this method were not pursued. Figure 2 shows the particle size distribution and zeta potential for the formulation prepared by using high-pressure homogenization.

Characterization of CCI-001 loaded albumin nanoparticle prepared by desolvation methods

The characteristics of the formulations prepared with the traditional desolvation method are shown in Table 3. This technique allowed the preparation of nanoparticles with smaller size (average hydrodynamic diameters < 150 nm), and a lower polydispersity index (<0.1). In this study, the nanoparticles produced by desolvation were more stable over time than the ones prepared by emulsification, and showed higher negative zeta potential values, between -26 and -30 mV. However, the entrapment efficiency of CCI-0001 was still low (between 2.9 and 3.6%) compared to the entrapment efficiency of drugs such as paclitaxel, docetaxel and doxorubicin encapsulated in the albumin nanocarrier (37,47,48,49).

The characteristics of the nanoparticles obtained by the modified desolvation method are presented in Table 4. The values of the hydrodynamic diameter, PDI and zeta potential are similar to those obtained by the traditional desolvation method. The only difference is that this optimized technique allowed higher encapsulation efficiency (between 5 and 8%, depending on the formulation) for CCI-001.

The size of the drug-loaded nanoparticles (optimal formulations, MD1 and MD7) obtained by the modified version of the desolvation method was not statistically different from that of blank BSA and HSA nanoparticles, respectively (Table 4), ($P > 0.05$). The zeta potential of the MD1 and MD7 formulations appeared to be more negative than that of the blank nanoparticles, although a statistically significant difference in zeta potential was only seen for the HSA-derived formulation (MD7) containing CCI-001 and the blank nanoparticles ($P < 0.05$). The particle size and zeta potential of the other formulation of drug-loaded HSA-derived nanoparticles (MD6) were significantly higher than those of drug-loaded nanoparticles prepared with BSA under the same pH conditions (MD1) ($P < 0.01$). However, when the pH of the HSA solution was increased prior to cross-linking (MD7), the difference in particle

diameter was diminished (Table 4). Size distribution and zeta potential of CCI-001-HSA nanoparticles (formulation MD7) prepared with modified desolvation method are presented in Figure 3.

Table 3. Characterization of the blank and CCI-001-loaded BSA nanoparticles produced by desolvation method. Data represent mean ± SD (n = 3).

Formulation	Hydrodynamic diameter (nm)	PDI	ZP (mV)	EE (%)	LC (%)
Blank	127.4 ± 13.2	0.08 ± 0.04	-23.1 ± 7.4	NA	NA
D1	142.5 ± 30.1	0.1 ± 0.05	-29.8 ± 2.3	3.2 ± 0.6	0.64 ± 0.12
D2	133.7 ± 25.5	0.08 ± 0.03	-27.6 ± 1.9	2.9 ± 1.3	0.26 ± 0.11
D3	113.2 ± 19.4	0.1 ± 0.03	-26.2 ± 2.6	3.6 ± 0.8	0.32 ± 0.07
D4	143.6 ± 18.6	0.08 ± 0.05	-30.2 ± 2.8	3.4 ± 0.3	0.16 ± 0.01

NA, not applicable; Hydrodynamic diameter (Z-average) measured by DLS; PDI, polydispersity index; ZP, zeta potential; EE, entrapment efficiency percent.

Table 4. Characterization of the blank and CCI-0001 loaded BSA and HSA nanoparticles produced by the modified desolvation method. Data represent mean ± SD (n = 3).

Formulation	Type of albumin	Hydrodynamic diameter (nm)	PDI	ZP (mV)	EE (%)	LC (%)
Blank	BSA	121.1 ± 5.2	0.04 ± 0.02	-21.9 ± 2.81	NA	NA
MD1	BSA	127.7 ± 4.9	0.04 ± 0.03	-25.7 ± 2.40	5.8 ± 0.7	0.53 ± 0.07 [g,h,i]
MD2	BSA	127.5 ± 9.6	0.03 ± 0.02	-26.0 ± 2.32	6.2 ± 1.1	0.39 ± 0.07
MD3	BSA	124 ± 13	0.05 ± 0.01	-28.5 ± 1.10 [a]	6.9 ± 0.89	0.26 ± 0.03
MD4	BSA	96.6 ± 3.4 [a,b,c,d,e]	0.04 ± 0.01	-29.2 ± 0.59 [a]	7.6 ± 1.1	0.15 ± 0.02
MD5	BSA	147 ± 21	0.10 ± 0.08	-29.8 ± 1.35 [a]	8.1 ± 0.4	0.16 ± 0.09
Blank	HSA	124.6 ± 3.7	0.03 ± 0.01	-23.4 ± 2.1	NA	NA
MD6	HSA	209.2 ± 4.5 [a,f]	0.03 ± 0.02	-28.3 ± 1.2 [a]	5.2 ± 0.6	0.47 ± 0.06
MD7	HSA	129.2 ± 3.8	0.03 ± 0.01	-29.6 ± 3.0 [a]	6.1 ± 0.9	0.56 ± 0.08

NA, not applicable; Hydrodynamic diameter (Z-average) measured by DLS; PDI, polydispersity index; ZP, zeta potential; EE, entrapment efficiency percent, LC, loading capacity. [a] Significantly different from the blank NPs in the same group, BSA- or HSA-derived ($P < 0.05$). [b] Significantly different from MD1 ($P < 0.05$), [c] Significantly different from MD2 ($P < 0.05$), [d] Significantly different from MD3 ($P < 0.05$), [e] Significantly different from MD5 ($P < 0.05$), [f] Significantly different from MD7 ($P < 0.05$). [g] Significantly different from MD3 ($P < 0.01$). [h] Significantly different from MD4 ($P < 0.01$). [i] Significantly different from MD5 ($P < 0.01$).

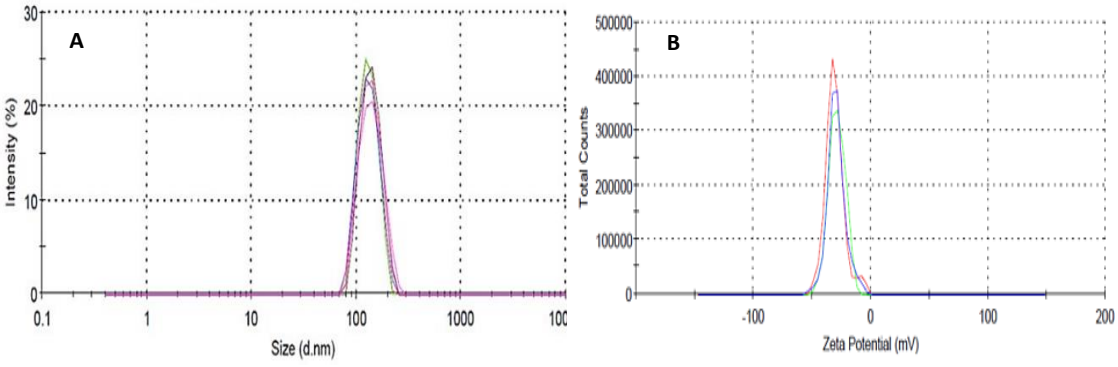

Figure 3. Representative particle size distribution (A) and zeta potential (B) diagram of CCI-001-loaded HSA nanoparticles (formulation MD7) prepared with modified desolvation method. Each coloured line represents one replicate of the same formulation.

Nanoparticle's morphology

SEM images (at 45000-fold and 16000-fold magnification) of CCI-001-loaded HSA nanoparticles and CCI-001-loaded BSA nanoparticles are shown in Figure 4. These images show a spherical morphology and relatively

uniform size for both HSA and BSA nanoparticles. The mean particle size obtained by DLS is in good agreement with those observed in SEM images.

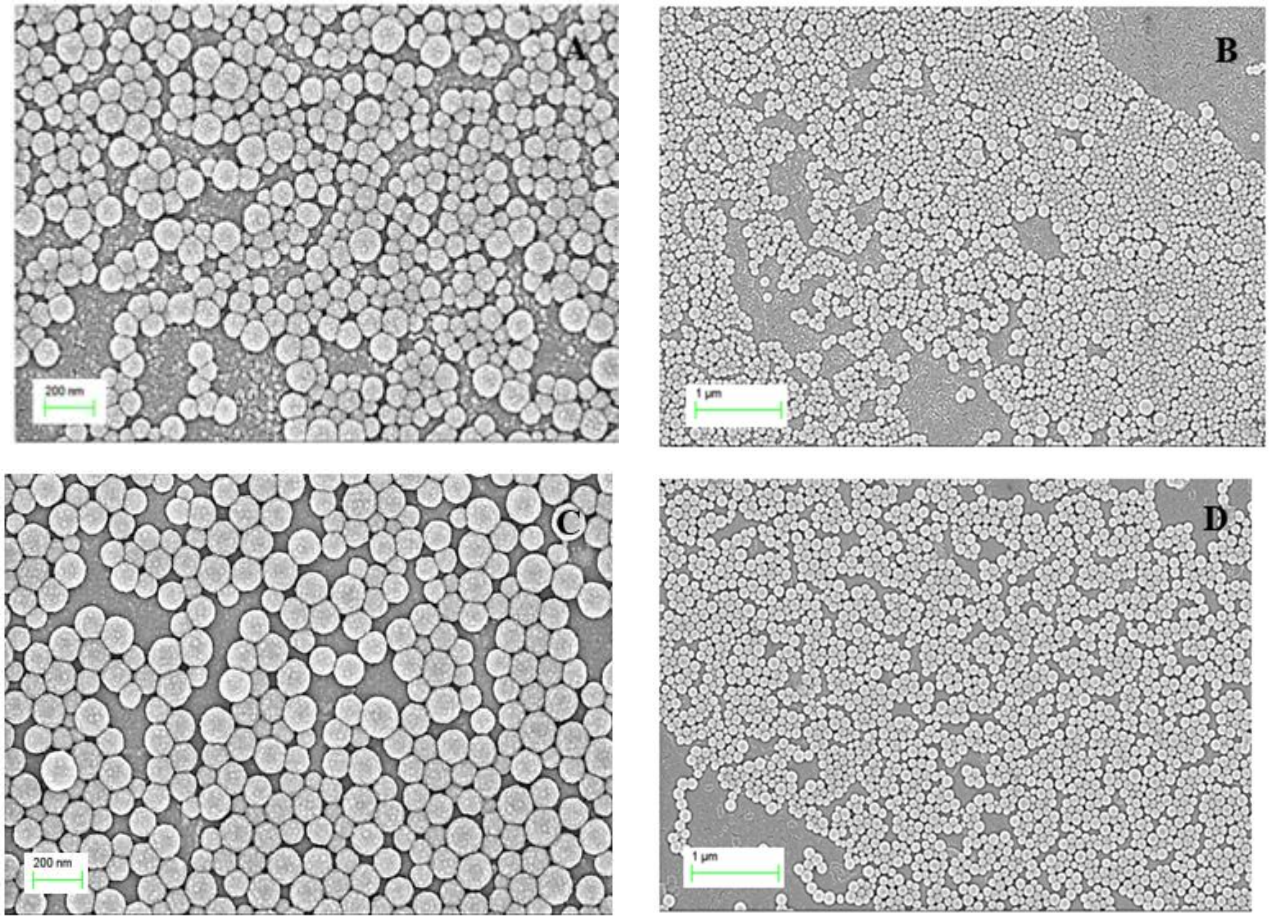

Figure 4. SEM images of (A) CCI-001-loaded BSA NPs (MD1) at 45k-fold magnification, and (B) 16k-fold magnification; (C) CCI-001-loaded HSA NPs (MD7) at 45k-fold magnification, and (D) 16k-fold magnification

In vitro drug release

Figure 5 shows the percent cumulative release of encapsulated CCI-001 from the albumin nanoparticles or from the ethanolic solution, as a function of time. The data showed a sustained release pattern over 24 hours for both BSA-NPs (MD1) and HSA-NPs (MD7) nanoparticles, without an initial burst release. On the other hand, the release of the free drug from the ethanolic solution through the dialysis membrane was fast, reaching 100% in less than 4 hours as all CCI-001 molecules are free in solution and they diffuse through the dialysis membrane much faster. The MRT values were 5.14 ± 0.33 h, 6.88 ± 0.15 h and 1.17 ± 0.15 h for BSA-NPs (MD1), HSA-NPs (MD7) and free drug, respectively. Therefore, the nanoparticle formulations (BSA and HSA, respectively) showed a 4.4- and 6-fold increase in the MRT values compared to free drug. A significant difference between the MRT of CCI-HSA NPs and CCI-BSA NPs was observed (P <0.01).

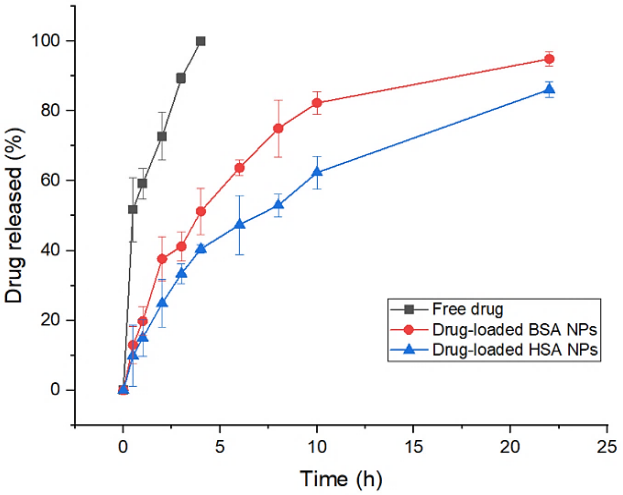

Figure 5. *In vitro*, CCI-001 release profiles for drug-loaded-BSA and -HSA nanoparticle formulations (MD1 and MD7, respectively) compared to free drug solution. Data represent Mean ± SD (n = 3).

The effect of cryoprotectant on the stability of CCI-001 loaded albumin nanoparticles

Table 5 illustrates the effects of trehalose addition on the size and zeta potential of the nanoparticles, following reconstitution of freeze-dried nanoparticles in double-distilled water. As the results show, the presence of a cryoprotectant was vital for a stable freeze-dried formulation and the lack of the cryoprotectant led to the aggregation of the nanoparticles. No significant differences were observed for hydrodynamic diameters and zeta potential of freeze-dried (with trehalose) drug-loaded HSA and BSA nanoparticles reconstituted in double-distilled water, compared with those of MD1 (drug-loaded BSA NPs) and MD7 (drug-loaded HSA NPs) formulations freshly prepared and initially used for freeze drying

Table 5. Influence of trehalose (2.5%) as cryoprotectant on the size of freeze-dried CCI-001 loaded albumin nanoparticles reconstituted in double-distilled water. Data represent mean ± SD (n = 3).

	Freeze-dried CCI-001-BSA NPs		**Freeze-dried CCI-001-HSA NPs**	
	With trehalose	**No trehalose**	**With trehalose**	**No trehalose**
Z average	131.6 ± 6.9 [a]	555.1 ± 19.3**	134.1 ± 4.2 [b]	579.9 ± 12.5**
Zeta potential	-21.7 ± 2.3 [a]	-10.2 ± 5.9*	-26.1 ± 3.4 [b]	-14.5 ± 5.2*

** Statistically different from the formulation with trehalose ($P < 0.01$). * Statistically different from the formulation with trehalose ($P < 0.05$). [a] No significant differences compared to MD1 (drug-loaded BSA NPs); [b] No significant differences compared to MD7 (drug-loaded HSA NPs) formulations freshly prepared and initially used for freeze drying (P>0.05) (Table 4).

Cytotoxicity of CCI-001 as free and HSA nanoparticle formulation in colorectal cancer cells

Figure 6 shows the cytotoxicity of the empty carrier, free drug and drug-loaded nanoparticles, against SW620 and HCT116 cells at 48 h (A & C) and at 72 h (B & D). The comparison between the IC_{50}s of CCI-001-loaded HSA nanoparticles and that of free CCI-001, at 48 and 72 hours in both cell lines is illustrated in Table 6. The results of the cell toxicity studies showed that the drug-loaded nanoparticles exhibited greater toxicity than free CCI-001 evidenced by lower IC_{50} of CCI-001 in NPs compared to free drug (Table 6). The SW620 cells appeared to be more sensitive to cytotoxic effects of CCI-001. Blank nanoparticles showed some cell toxicity, at high concentrations and longer incubation times (Figure 6), which may be attributed to the presence of free cross-linker

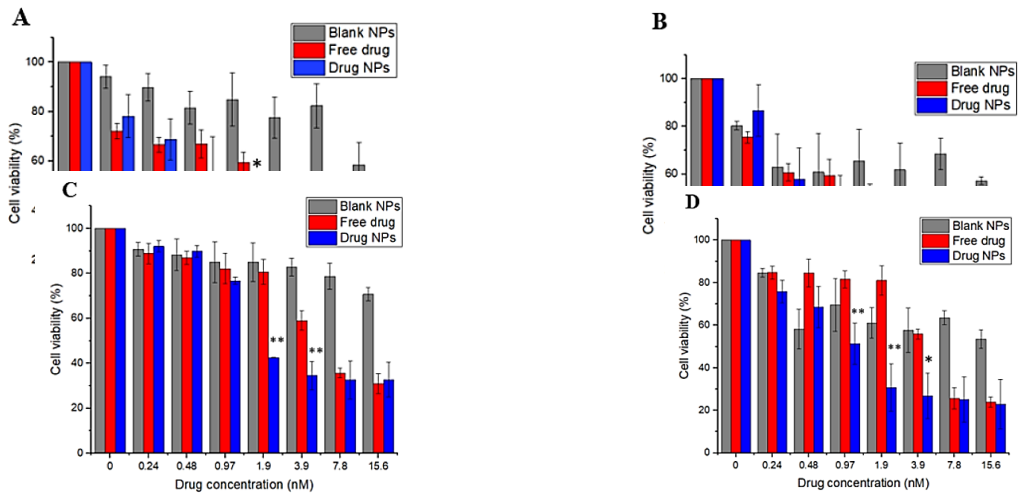

Figure 6. Comparison between the cytotoxicity of blank NPs, free CCI-001 and CCI-001-loaded HSA NPs in SW620 at (A) 48 h and (B) 72 h, and in HCT116 at (C) 48 h and (D) 72 h. Data represent Mean ± SD (n=3). *Statistically different from the free drug ($P < 0.05$). **Statistically different from the free drug ($P < 0.01$)

Table 6. IC_{50}s (nM) of CCI-001-loaded HSA nanoparticles and free CCI-001, in SW620 and HCT116 cancer cell lines, at 48 and 72 hours. Data represent mean ± SD (n = 3).

	SW-620		**HCT-116**	
Time	**Free drug**	**Drug NPs**	**Free drug**	**Drug NPs**
48 h	2.36 ± 0.32	1.08 ± 0.57*	4.39 ± 0.27	1.27 ± 0.21**
72 h	2.06 ± 0.29	0.62 ± 0.31**	4.24 ± 0.20	0.9 ± 0.1**

* Statistically different from the free drug ($P < 0.05$). ** Statistically different from the free drug ($P < 0.01$)

DISCUSSION

The main objective of this study was to develop albumin nanoparticle formulations of CCI-001 (Figure 1) that can potentially reduce the nonspecific toxicity of this novel β-III tubulin inhibitor in the treatment of paclitaxel-resistant tumours. This was shown to be a challenging task, given the high lipophilicity and low water solubility of the novel chemotherapeutic agent CCI-001 (< 0.007 mg/mL). Here, we investigated emulsification by sonication and high-pressure homogenization, desolvation and a modified desolvation method for loading of CCI-001 into albumin nanoparticles from bovine and human origin at different drug-to-SA ratios and with two solvents, ethanol and acetone (Table 1 and 2). The physicochemical characteristics of the developed nanoparticles were then assessed. The goal was to develop reproducible particles in a nanometer size range, with a low tendency for aggregation, sufficiently high encapsulation of CCI-001 allowing the *in vivo* use, and relatively slow drug release. Previous studies have reported successful encapsulation of hydrophobic drugs into albumin-based nanoparticles using the above-mentioned techniques (31,46,50).

Emulsifications by high pressure homogenization is one of the most popular techniques to generate drug-loaded albumin nanoparticles (51,52). This method takes advantage of the tendency of hydrophobic drugs in an o/w emulsion to interact with albumin in water upon evaporation of the organic solvent (53). In previous studies, Hosseinifar et al (54) have investigated the use of both sonicator as well as high-pressure homogenization on the physicochemical properties of HSA nanoparticles. In agreement with their results, we have found the use of high-pressure homogenization to be more reliable and effective than sonication in achieving BSA nanoparticles of smaller diameters (Figure 4). However, the nanoparticles produced by emulsification methods, as previously mentioned, showed aggregation upon storage, reaching hydrodynamic diameters of around 800 nm in a day after the production. Furthermore, the encapsulation efficiency and loading capacity of CCI-001 were too low (< 3% and 2% for sonication and high-pressure homogenization, respectively). Sonication at higher energies, use of smaller sample volumes, change in the type of organic solvent, and modulation of albumin/drug ratios were just tried and did not improve the physicochemical characteristics of albumin nanoparticles prepared by the emulsion method (data not shown).

Desolvation is a known method to produce albumin nanoparticles (55,56). In the current study, the use of the desolvation method allowed the preparation of more reproducible albumin nanoparticles of proper size and zeta potential. Furthermore, the nanoparticles were more stable over time, not showing as much tendency for aggregation compared to nanoparticles prepared by the emulsification method. In fact, the hydrodynamic diameters and zeta potential values of the obtained formulations, measured over several consecutive days, remained fairly constant over time. However, the low encapsulation efficiency of CCI-001 (< 4%) implied further need for the modification and optimization of the desolvation technique (Table 3). As altering the drug to albumin ratio (formulations D1, D2 and D4) or choice of the organic phase (formulation D3) did not make a significant impact on the encapsulation efficiency of CCI-001 in albumin nanoparticles prepared by the traditional desolvation method (41), we tried incubation of the drug with preformed and cross-linked albumin nanoparticles. This led to the development of nanoparticles (formulations MD1 and MD7) with narrow size distribution, negative zeta potential and, higher CCI-001 encapsulation efficiency (Table 4) compared to the other two previously

described techniques. high-pressure homogenization and traditional desolvation. It is suggested that the CCI-001 had a greater chance over time to enter the already prepared crosslinked albumin nanoparticles during the modified desolvation method.

Furthermore, we investigated the effect of different parameters in the modified desolvation method on the properties of CCI-001-loaded BSA or HSA nanoparticles. The optimal ethanol to water ratio was found to be 1 to 4, leading to higher CCI-001 encapsulation. Drug to BSA ratios of 1/10, 1/15, 1/25 and 1/50 were tested. The results showed a positive trend in loaded drug levels and initial drug to BSA ratios, although the differences were not statistically significant. The loading capacity of the drug was considerably increased by reducing the albumin concentration (statistical difference from MD3, MD4 and MD5, $P<0.01$, Table 4). Although the overall effect of albumin concentration on the size or the zeta potential of BSA nanoparticles was not significant, the MD4 formulation prepared at 1 to 50 BSA: CCI-001 ratio showed significantly smaller particle diameter compared to all the other formulations in the same group (BSA-derived NPs). This result is in agreement with previous studies where albumin nanoparticles were prepared by the nanoprecipitation method (57,58).

Overall, the results showed that the modified desolvation method using a drug to albumin w/w ratio of 1 to 10 led to the production of BSA nanoparticles with appropriate size, zeta potential and highest drug loading compared to the other methods. For this reason, the same formulation condition was used to prepare HSA nanoparticle formulations of CCI-001. The results showed both BSA and HSA nanoparticle formulations of CCI-001 to be spherical, homogeneous and uniform in diameter (Figure 4). Both were characterized by average hydrodynamic diameters of around 125-130 nm and a zeta potential of around -30 mV. The negative surface charges of both blank and drug-loaded nanoparticles were expected due to the negative charge of albumin at the examined pH values of 8 and 9 (59).

The pH value of the albumin solution prior to ethanol addition strongly influenced the resulting particle size. At greater pH, particle diameter was significantly reduced i.e., from 147.5 nm (MD5) at pH 7 to 96.6 nm (MD4) at pH of 8 to for BSA nanoparticles. Similarly, for HSA nanoparticles, when the pH of the solution was increased from 8 to the higher pH value (MD7), the particle size was reduced from 209.2 nm to 129.2 nm. This observation is in line with the previous work that used the same approach to prepare colloidal albumin nanoparticles (57,60). As suggested by Langer et al (57), at increasing pH values, the particle size of HSA-derived nanoparticles was reduced, apparently due to an increase in the ionization of the HSA (isoelectric point of around 4.7-5), which leads to the repulsion of HSA molecules, avoiding aggregates during particle formation.

Interestingly, nanoparticles based on HSA generated larger particles (209.2 ± 4.5 nm, MD6) compared to the nanoparticles obtained from BSA (127.7 ± 4.9 nm, MD1) under the same preparation conditions (Table 4). The exact reason for the bigger size of HSA compared to BSA nanoparticles, obtained under the same preparation conditions, is not well understood. It is known that HSA and BSA share 80% sequence homology, their molecular weights differ by less than 1%, and their isoelectric points are identical. Nevertheless, the finding obtained in this study is in agreement with the work conducted by Tazhbayev et al (61), who demonstrated that the average particle size of BSA-derived nanoparticles (167 ± 5 nm) was smaller than that of HSA-derived nanoparticles (216 ± 9 nm).

Taking into account all particle characteristics of different modified desolvation (MD) formulations prepared and evaluated in the current study, the formulations MD1 and MD7 (Table 4) were used for subsequent cryoprotection, *in vitro* release and cell toxicity evaluations. In agreement with the results obtained by Qu et al (62), when used as cargo in the nanoparticle formulation, the drug required a longer time to be released and that is generally due to the gradual diffusion from the stable matrix of the albumin nanoparticles. However, in this study, the release from the HSA nanoparticles was fairly faster (MRT~7 h, complete release, 24 h), compared to the release profiles obtained in many previous studies that investigated the characteristics of drug-loaded albumin nanoparticles (41,56,63,64,65). This may reflect the loose interaction of CCI-001 with albumin nanoparticles.

Hu et al (66) investigated the interaction between colchicine, the parent compound from which CCI-001 is derived, and HSA by fluorescence and UV-Vis absorption spectroscopy. The results exhibited the spontaneous formation of colchicine-HSA complexes with moderate binding affinity, where Van der Waals interactions and hydrogen bonds played a vital role in the stability of the complex. In particular, binding and molecular docking studies have shown that the binding site for colchicine on SA is located in sub-

domain IIA (Trp^{214}) (67). However, in vitro, studies have shown that the binding of colchicine to albumin is low to moderate at 40% in a nonsaturable manner. Negligible amounts also bind to acid α1-glycoprotein, γ-globulins, and lipoproteins (68). Although the extent of CCI-001 binding to albumin has not yet been studied, molecular docking simulation studies conducted by Dr. Tuszynski's group (see the Supplementary Material) have shown that CCI-001 seems to bind near tryptophan, as the parent compound colchicine, but the location is slightly different. Even though several studies investigated the nature of the interactions between colchicine (the drug from which CCI-001 is derived) and SA (66,67,68), to the best of our knowledge no formulations based on colchicine-loaded albumin-nanocarrier have been reported in the literature.

Interestingly, the release rate of CCI-001 from HSA-NP was significantly slower than that of BSA-NPs (MRT, 6.88 ± 0.15 h *vs* 5.14 ± 0.33 h) (Figure 5). Although HSA and BSA are highly homologous in terms of amino acid sequences, the two albumins show different structural orientations and dynamics. A different number of aromatic residues in HSA and BSA located in subdomains IIA may affect the binding properties of aromatic ligands which binds to the binding site I located on this subdomain. In addition, BSA has a rigid and compact structure owing to the highest number of intra hydrogen bonds, whilst HSA displays a more flexible and mobile structure (69). Binding parameters of typical site II (situated on IIIA subdomain) binding drugs on different albumins including HSA and BSA showed higher binding constants for HSA compared to BSA which could be best explained by microenvironmental changes in the binding sites resulting from a change in the size and/or hydrophobicity of the binding pocket (70). These features may explain the higher affinity and EE of the lipophilic CCI-001 to HSA compared to BSA and the slower release of the compound from HSA. Although further studies on the binding site of CCI-001 on BSA are required before making definitive conclusions.

The BSA and HSA nanoparticles (MD1 and MD7 formulations) were then freeze-dried with and without trehalose as cryoprotectant and reconstituted to evaluate the effect of cryoprotection on the size of reconstituted nanoparticles. In the absence of trehalose, freeze-drying caused significant nanoparticle aggregation which led to a greater than four folds increase in the particle size ($P < 0.01$) and an increase in the zeta potential ($P < 0.05$), (Table 5). Previous studies have shown that trehalose, used to prevent particle growth and aggregation, has been very effective as a cryoprotectant (71). In the presence of trehalose, no significant differences were observed for z-average and zeta potential of both HSA and BSA freeze-dried nanoparticles reconstituted in double-distilled water, compared with those of MD1 and MD7 formulations freshly prepared and initially used for freeze drying. Both BSA- and HSA-derived NPs showed a similar size and zeta potential reduction in response to the addition of the cryoprotectant. The results were in agreement with the findings reported by Almalik et al (72), who demonstrated that albumin nanoparticles lyophilized without cryoprotectants showed an increase in average size, due to high agglomeration. Freeze-drying removes water from a frozen sample through sublimation. The process consists of freezing, primary drying (ice sublimation) and secondary drying (desorption of unfrozen water) (73). To protect nanoparticles from stress and aggregation, a cryoprotectant (in this case, trehalose) is generally used. When a cryoprotectant is present, water freezes into ice crystals while excluding solutes and particles into a cryo-concentrated liquid phase. Trehalose, a naturally derived sugar, protects the protein from cryopreservation damage (74). The coating of trehalose, which "entraps" the protein, slows down the water molecules directly adjacent to the albumin, preventing ice crystallization in its immediate vicinity. For this reason, its role is fundamental, since the interaction between water and the protein could dramatically affect the protein structure, dynamics and functionality (71).

Cytotoxicity studies against two colorectal cancer cell lines (SW620 and HCT116) showed the higher activity of CCI-001-loaded HSA nanoparticles compared to the free drug. This can be explained by better cellular interaction of CCI-001 by its albumin nanocarrier due to higher drug solubilization, stabilization or cellular uptake (75,76). However, the presence of free glutaraldehyde as the crosslinking agent in nanoparticle samples could have partially contributed to this observation, as well (77). Overall, CCI-001 was shown to be a very potent anticancer agent as free drug and as a component of HSA nanoparticle formulations (IC_{50}s in the range of nM). Since the IC_{50} values for CCI-001 on the tested cell lines are very low (≈ 1 nM = 0.5 ng/mL), the drug-loaded nanoparticle formulations (MD1 to MD7) could lead to aqueous drug concentrations up to 25,000 times higher than the IC_{50} of the compound. This indicates that although loading capacity is very low, still a reasonable quantity of formulations can be used to achieve

relevant drug concentrations in preclinical *in vivo* studies.

CONCLUSIONS

A modified desolvation technique using drug incubation with preformed cross-linked BSA as well as HSA nanoparticles was shown to be the best method for the preparation of albumin nanoparticle formulations of a novel and potent β–tubulin inhibitor, CCI-001. The albumin nanoparticles were able to maintain or enhance the potency of encapsulated CCI-001 against colorectal cancer cell lines while making the drug release slower, *in vitro*. Despite the low drug content level in the HSA nanoparticles of CCI-001, the formulation provides relevant concentrations for further *in vivo* studies in animal models due to high drug potency.

ACKNOWLEDGMENTS

The authors acknowledge both financial and material support received from the Allard Foundation. We thank the Faculty of Engineering, University of Alberta, for assistance with the SEM images. High-pressure homogenization was performed at the University of Alberta, Faculty of Agricultural, Life and Environmental Sciences. J.A. T. acknowledges funding for this research received from NSERC (Canada)

REFERENCES

1. Bray F, Ferlay J, Soerjomataram I, Siegel RL, Torre LA, Jemal A. Global cancer statistics 2018: GLOBOCAN estimates of incidence and mortality worldwide for 36 cancers in 185 countries. CA Cancer J Clin. 2018, 68(6): 394–424. Doi: 10.3322/caac.21492.
2. Senapati S, Mahanta AK, Kumar S, Maiti P. Controlled drug delivery vehicles for cancer treatment and their performance. Signal Transduct Target Ther. 2018, 3:7. Doi:10.1038/s41392-017-0004-3.
3. Navya PN, Kaphle A, Srinivas SP, Bhargava SK, Rotello VM, Daima HK. Current trends and challenges in cancer management and therapy using designer nanomaterials. Nano Convergence. 2019, 6(23). doi.org/10.1186/s40580-019-0193-2.
4. Patra JK, Das G, Fraceto LF, Campos EVR, Rodriguez-Torres MP, Acosta-Torres LS, DiazTorres LA, Grillo R, Swamy MK, Sharma S, Habtemariam S, Shin HS. Nano based drug delivery systems: recent developments and future prospects. J Nanobiotechnol. 2018, 16(71). doi.org/10.1186/s12951-018-0392-8.
5. Amini MA, Ahmed T, Liu FC, Abbasi AZ, Soeandy CD, Zhang RX, Prashad P, Cummins CL, Rauth AM, Henderson JT, Wu XY. Exploring the transformability of polymer-lipid hybrid nanoparticles and nanomaterial-biology interplay to facilitate tumor penetration, cellular uptake and intracellular targeting of anticancer drugs. Expert Opinion on Drug Delivery. 2021, 29:1-4.
6. Bueno O, Estévez Gallego J, Martins S, Prota AE, Gago F, Gomez-SanJuan A, Camarasa M-J, Barasoain I, Steinmetz MO, Diaz F, Pérez-Pérez M-J, Liekens S, Priego E-M. High-affinity ligands of the colchicine domain in tubulin based on a structure-guided design. Sci Rep. 2018, 8**:**4242. Doi: 10.1038/s41598-018-22382-x.
7. Spasevska I, Ayoub AT, Winter P, Preto J, Wong GK, Dumontet C, Tuszynski JA. Modeling the Colchicum autumnale Tubulin and a Comparison of Its Interaction with Colchicine to Human Tubulin. Int J Mol Sci. 2017, 18(8): 1676. Doi: 10.3390/ijms18081676.
8. Lu Y, Chen J, Xiao M, Li W, Miller DD. An overview of tubulin inhibitors that interact with the colchicine binding site. Pharm Res. 2012, 29(11): 2943–2971. Doi: 10.1007/s11095-012-0828-z.
9. Majcher U, Klejborowska G, Moshari M, Maj E, Wietrzyk J, Bartl F, Tuszynski JA, Huczyński A. Antiproliferative Activity and Molecular Docking of Novel Double-Modified Colchicine Derivatives. Cells. 2018, 7(11): 192. Doi: 10.3390/cells7110192.
10. Akhmanova A, Steinmetz MO. Tracking the ends: a dynamic protein network controls the fate of microtubule tips. Nat Rev Mol Cell Biol. 2008, 9(4): 309–322. Doi: 10.1038/nrm2369.
11. Brouhard GJ, Rice LM. Microtubule dynamics: an interplay of biochemistry and mechanics. Nat Rev Mol Cell Biol. 2018, 19(7): 451–463. Doi: 10.1038/s41580-018-0009-y.
12. Gan PP, McCarroll JA, Po'uha T, Kamath K, Jordan MA, Kavallaris M. Microtubule dynamics, mitotic arrest, and apoptosis:

drug-induced differential effects of βIII-tubulin. Mol Cancer Ther. 2020, 9(5): 1339-1348. 10.1158/1535-7163.MCT-09-0679.
13. AbouAitah K, Hassan HA, Swiderska-Sroda A, Gohar L, Shaker OG, Wojnarowicz J, et al. Targeted Nano-Drug Delivery of Colchicine against Colon Cancer Cells by Means of Mesoporous Silica Nanoparticles. Cancers (Basel). 2020, 12(1): 144. Doi: 10.3390/cancers12010144.
14. Patterson DM, Rustin GJS. Vascular Damaging Agents. Clinical Oncology. 2007, 19(6): 443-456. Doi: 10.1016/j.clon.2007.03.014.
15. Kesselheim AS, Franklin JM, Kim SC, Seeger JD, Solomon DH. Reductions in Use of Colchicine after FDA Enforcement of Market Exclusivity in a Commercially Insured Population. J Gen Intern Med. 2015, 30(11): 1633–1638. Doi: 10.1007/s11606-015-3285-7.
16. Patent https://patents.google.com/patent/US9458101?oq=tuszynski+colchcicine.
17. Slobodnick A, Shah B, Pillinger MH, Krasnokutsky S. Colchicine: old and new. Am J Med. 2015, 128(5): 461–470. Doi: 10.1016/j.amjmed.2014.12.010.
18. Finkelstein Y, Aks SE, Hutson JR, Juurlink DN, Nguyen P, Dubnov-Raz G, et al. Colchicine poisoning: the dark side of an ancient drug. Clin Toxicol (Phila). 2010, 48(5): 407–414. Doi: 10.3109/15563650.2010.495348.
19. Maxwell MJ, Muthu P, Pritty PE. Accidental colchicine overdose. A case report and literature review. Emerg Med J. 2002, 19(3): 265-267. Doi: 10.1136/emj.19.3.265.
20. Mukhtar E, Adhami VM, Mukhtar H. Targeting microtubules by natural agents for cancer therapy. Mol Cancer Ther. 2014, 13(2): 275–284. Doi: 10.1158/1535-7163.MCT-13-0791.
21. Stengel C, Newman S, Leese MP, Potter BVL, Reed MJ, Purohit A. Class III *β*-tubulin expression and *in vitro* resistance to microtubule targeting agents. Br J Cancer. 2010, 102: 316–324. Doi: 10.1038/sj.bjc.6605489.
22. Wang RC, Chen X, Parissenti AM, Joy AA, Tuszynski J, Brindley DN, Wang Z. Sensitivity of docetaxel-resistant MCF-7 breast cancer cells to microtubule-destabilizing agents including vinca alkaloids and colchicine-site binding agents. PloS One. 2017, 12(8): e0182400. Doi: 10.1371/journal.pone.0182400.
23. Johnson L, Goping IS, Rieger A, Mane JY, Huzil T, Banerjee A, Luduena R, Hassani B, Winter P, Tuszynski JA. Novel colchicine derivatives and their anti-cancer activity. *Curr Top Med Chem. 2017, 17*(22): 2538-2558. Doi: 10.2174/1568026617666170104143618.
24. Torin Huzil J, Winter P, Johnson L, Weis AL, Bakos T, Banerjee A, Luduena RF, Damaraju S, Tuszynski JA. Computational design and biological testing of highly cytotoxic colchicine ring A modifications. Chem Biol Drug Des. 2010, 75(6): 541–550. Doi: 10.1111/j.1747-0285.2010.00970.x.
25. Narvekar M, Xue HY, Eoh JY, Wong HL. Nanocarrier for poorly water-soluble anticancer drugs—barriers of translation and solutions. Aaps Pharmscitech. 2014, 15(4): 822-33.
26. A Study of CCI-001 in Patients With Recurrent and/or Metastatic Solid Tumours - Full Text View - ClinicalTrials.gov
27. Spada A, Emami J, Tuszynski JA, Lavasanifar A. The uniqueness of albumin as a carrier in nano-drug delivery. Mol Pharm. 2021, 18(5): 1862-1894.
28. Tang X, Wang G, Shi R, Jiang K, Meng L, Ren H, Wu J, Hu Y. Enhanced tolerance and antitumor efficacy by docetaxel-loaded albumin nanoparticles. Drug deliv. 2016, 23(8): 2686–2696. Doi: 10.3109/10717544.2015.1049720.
29. Lee JH, Moon H, Han H, Lee IJ, Kim D, Lee HJ, Ha SW, Kim H, Chung JW. Antitumor Effects of Intra-Arterial Delivery of Albumin-Doxorubicin Nanoparticle Conjugated Microbubbles Combined with Ultrasound-Targeted Microbubble Activation on VX2 Rabbit Liver Tumors. Cancers (Basel). 2019, 11(4): 581. Doi: 10.3390/cancers11040581.
30. Park CR, Jo JH, Song MG, Park JY, Kim YH, Youn H, Paek SH, Chung JK, Jeong JM, Lee YS, Kang KW. Secreted protein acidic and rich in cysteine mediates active targeting of human serum albumin in U87MG xenograft mouse models. Theranostics. 2019, 9(24): 7447–7457. Doi: 10.7150/thno.34883.
31. Green MR, Manikhas GM, Orlov S, Afanasyev B, Makhson AM, Bhar P, Hawkins MJ. Abraxane, a novel Cremophor-free, albumin-bound particle form of

paclitaxel for the treatment of advanced non-small-cell lung cancer. Ann Oncol. 2006, 17(8): 1263–1268. Doi: 10.1093/annonc/mdl104.

32. Ibrahim NK, Desai N, Legha S, Soon-Shiong P, Theriault RL, Rivera E, Esmaeli B, Ring SE, Bedikian A, Hortobagyi GN, Ellerhorst JA. Phase I and pharmacokinetic study of ABI-007, a Cremophor-free, protein-stabilized, nanoparticle formulation of paclitaxel. Clin Cancer Res. 2002, 8(5):1038-44.
33. Fu Q, Sun J, Zhang W, Sui X, Yan Z, He Z. Nanoparticle albumin-bound (NAB) technology is a promising method for anti-cancer drug delivery. Recent Pat Anticancer Drug Discov. 2009, 4(3): 262–272. Doi: 10.2174/157489209789206869.
34. Li C, Li Y, Gao Y, Wei N, Zhao X, Wang C, Li Y, Xiu X, Cui J. Direct comparison of two albumin-based paclitaxel-loaded nanoparticle formulations: is the crosslinked version more advantageous? Int J Pharm. 2014, 468(1-2): 15–25. Doi: 10.1016/j.ijpharm.2014.04.010.
35. Mahdi Jafari S, He Y, Bhandari B. Nano-Emulsion Production by Sonication and Microfluidization—A Comparison. International Journal of Food Properties. 2006, 9(3): 475-485. Doi: 10.1080/10942910600596464.
36. Taha A, Ahmed E, Ismaiel A, Ashokkumar M, Xu X, Pan S, Hu H. Ultrasonic emulsification: An overview on the preparation of different emulsifiers-stabilized emulsions. Trends in Food Science & Technology. 2020, 105: 363-377. Doi: 10.1016/j.tifs.2020.09.024.
37. Kim B, Lee C, Lee ES, Shin BS, Youn YS. Paclitaxel and curcumin co-bound albumin nanoparticles having antitumor potential to pancreatic cancer. Asian Journal of Pharmaceutical Sciences. 2016, 11(6): 708-814.
38. Wang Z, Li Z, Zhang D, Miao L, Huang G. Development of etoposide-loaded bovine serum albumin nanosuspensions for parenteral delivery. Drug Deliv. 2015, 22(1): 79-85.
39. Jahanban-Esfahlan A, Dastmalchi S, Davaran S. A simple improved desolvation method for the rapid preparation of albumin nanoparticles. Int J Biol Macromol. 2016, 91: 703–709. Doi: 10.1016/j.ijbiomac.2016.05.032.
40. Kimura K, Yamasaki K, Nakamura H, Haratake M, Taguchi K, Otagiri M. Preparation and in Vitro Analysis of Human Serum Albumin Nanoparticles Loaded with Anthracycline Derivatives. Chemical & pharmaceutical bulletin. 2018, 66(4): 382–390. Doi: 10.1248/cpb.c17-00838.
41. Merodio M, Arnedo A, Renedo MJ, Irache JM. Ganciclovir-loaded albumin nanoparticles: characterization and in vitro release properties. Eur J Pharm Sci. 2001, 12(3): 251-9. Doi: 10.1016/s0928-0987(00)00169-x.
42. Abdelwahed W, Degobert G, Stainmesse S, Fessi H. Freeze-drying of nanoparticles: formulation, process and storage considerations. Adv Drug Deliv Rev. 2006, 58(15): 1688–1713. Doi: 10.1016/j.addr.2006.09.017.
43. Anhorn MG, Mahler HC, Langer K. Freeze drying of human serum albumin (HSA) nanoparticles with different excipients. Int J Pharm. 2008, 363(1-2): 162–169. Doi: 10.1016/j.ijpharm.2008.07.004.
44. Katas H, Hussain Z, Rahman SA. Storage Stabilisation of Albumin-Loaded Chitosan Nanoparticles by Lyoprotectants. Trop J Pharm Res. 2013, 12(2): 135-142. Doi: 10.4314/tjpr.v12i2.1.
45. Borenfreund E, Babich H, Martin-Alguacil N, Comparisons of two in vitro cytotoxicity assays – the neutral red (NR) and tetrazolium MTT tests. Toxicology in vitro. 1988, 2(1): 1-6. doi.org/10.1016/0887-2333(88)90030-6
46. Salehiabar M, Nosrati H, Javani E, Aliakbarzadeh F, Kheiri Manjili H, Davaran S, Danafar H. Production of biological nanoparticles from bovine serum albumin as controlled release carrier for curcumin delivery. Int J Biol Macromol. 2018, 115: 83–89. Doi: 10.1016/j.ijbiomac.2018.04.043.
47. Qu N, Sun Y, Li Y, Hao F, Qiu P, Teng L, Xie J, Gao Y. Docetaxel-loaded human serum albumin (HSA) nanoparticles: synthesis, characterization, and evaluation. BioMed Eng OnLine. 2019, 18:11. Doi: 10.1186/s12938-019-0624-7.
48. Honary S, Jahanshahi M, Golbayani P, Ebrahimi P, Ghajar K. Doxorubicin-loaded albumin nanoparticles: formulation and characterization. J Nanosci Nanotechnol. 2010, 10(11): 7752–7757. Doi: 10.1166/jnn.2010.2832.

49. Yi X, Lian X, Dong J, Wan Z, Xia C, Song X, Fu Y, Gong T, Zhang Z. Co-delivery of Pirarubicin and Paclitaxel by Human Serum Albumin Nanoparticles to Enhance Antitumor Effect and Reduce Systemic Toxicity in Breast Cancers. Mol Pharm. 2015, 12(11): 4085–4098. Doi: 10.1021/acs.molpharmaceut.5b00536.
50. Maryam K, Shakeri S, Kiani K. Preparation and in vitro investigation of antigastric cancer activities of carvacrol-loaded human serum albumin nanoparticles. IET Nanobiotechnol. 2015, 9(5): 294–299. Doi: 10.1049/iet-nbt.2014.0040.
51. Cortes J, Saura C. Nanoparticle albumin-bound (nab™)-paclitaxel: improving efficacy and tolerability by targeted drug delivery in metastatic breast cancer. EJC Supplements. 2018, 8(1): 1-10. Doi: 10.1016/S1359-6349(10)70002-1.
52. Cucinotto I, Fiorillo L, Gualtieri S, Arbitrio M, Ciliberto D, Staropoli N, Grimaldi A, Luce A, Tassone P, Caraglia M, Tagliaferri P. Nanoparticle albumin bound Paclitaxel in the treatment of human cancer: nanodelivery reaches prime-time? J Drug Deliv. 2013: 905091. Doi: 10.1155/2013/905091.
53. Lomis N, Westfall S, Farahdel L, Malhotra M, Shum-Tim D, Prakash S. Human Serum Albumin Nanoparticles for Use in Cancer Drug Delivery: Process Optimization and In Vitro Characterization. Nanomaterials (Basel). 2016, 6(6): 116. Doi: 10.3390/nano6060116.
54. Hosseinifar N, Sharif AAM, Goodarzi N, Amini M, Dinarvand R. Preparation of human serum albumin nanoparticles using a chemometric technique. J Nanostruct Chem. 2017, 7: 327–335. Doi: 10.1007/s40097-017-0242-5.
55. Storp B. Engel A, Boeker A, Ploeger M, Langer K. Albumin nanoparticles with predictable size by desolvation procedure. J Microencapsulation. 2012, 29(2): 138-146. Doi: 10.3109/02652048.2011.635218.
56. Zhao D, Zhao X, Zu Y, Li J, Zhang Y, Jiang R, Zhang Z. Preparation, characterization, and in vitro targeted delivery of folate-decorated paclitaxel-loaded bovine serum albumin nanoparticles. Int J Nanomedicine. 2010, 5: 669–677. Doi: 10.2147/ijn.s12918.
57. Langer K, Balthasar S, Vogel V, Dinauer N, von Briesen H, Schubert D. Optimization of the preparation process for human serum albumin (HSA) nanoparticles. Int J Pharm. 2003, 257(1-2): 169–180. Doi: 10.1016/s0378-5173(03)00134-0.
58. Tarhini M, Benlyamani I, Hamdani S, Agusti G, Fessi H, Greige-Gerges H, Bentaher A, Elaissari A. Protein-Based Nanoparticle Preparation via Nanoprecipitation Method. Materials (Basel). 2018, 11(3): 394. Doi: 10.3390/ma11030394.
59. Wiig H, Kolmannskog O, Tenstad O, Bert JL. Effect of charge on interstitial distribution of albumin in rat dermis in vitro. J Physiol. 2003, 550(Pt2): 505–514. Doi: 10.1113/jphysiol.2003.042713.
60. Lin W, Coombes AG, Davies MC, Davis SS, Illum L. Preparation of sub-100 nm human serum albumin nanospheres using a pH-coacervation method. J Drug Target. 1993, 1(3): 237–243. Doi: 10.3109/10611869308996081.
61. Tazhbayev Y, Mukashev O, Burkeyev M, Lozinsky VI. Synthesis and Comparative Study of Nanoparticles Derived from Bovine and Human Serum Albumins. Polymers. 2020, 12(6): 1301. Doi: 10.3390/polym12061301.
62. Qu N, Sun Y, Li Y, Hao F, Qiu P, Teng L, Xie J, Gao Y. Docetaxel-loaded human serum albumin (HSA) nanoparticles: synthesis, characterization, and evaluation. BioMed Eng OnLine. 2019, 18:11. Doi: 10.1186/s12938-019-0624-7.
63. Zhou G, Jin X, Zhu P, Yao JU, Zhang Y, Teng L, Lee RJ, Zhang X, Hong W. Human Serum Albumin Nanoparticles as a Novel Delivery System for Cabazitaxel. Anticancer research. 2016, 36(4): 1649–1656.
64. Honary S, Jahanshahi M, Golbayani P, Ebrahimi P, Ghajar K. Doxorubicin-loaded albumin nanoparticles: formulation and characterization. J Nanosci Nanotechnol. 2010, 10(11): 7752–7757. Doi: 10.1166/jnn.2010.2832.
65. Yi X, Lian X, Dong J, Wan Z, Xia C, Song X, Fu Y, Gong T, Zhang Z. Co-delivery of Pirarubicin and Paclitaxel by Human Serum Albumin Nanoparticles to Enhance Antitumor Effect and Reduce Systemic Toxicity in Breast Cancers. Mol Pharm. 2015, 12(11): 4085–4098. Doi: 10.1021/acs.molpharmaceut.5b00536.
66. Hu YJ, Liu Y, Zhao RM, Qu SS. Interaction of colchicine with human serum albumin investigated by spectroscopic methods. Int J

Biol Macromol. 2005, 37(3): 122–126. Doi: 10.1016/j.ijbiomac.2005.09.007.
67. Rabbani N, Tabrez S, Islam B, rehman MT, Alsenaidy AM, Alajmi MF, Khan RA, Alsenaidy MA, Khan MS. Characterization of colchicine binding with normal and glycated albumin: In vitro and molecular docking analysis. Journal of Biomolecular Structure and Dynamics. 2017, 3453-3462. doi.org/10.1080/07391102.2017.1389661.
68. Niel E, Scherrmann JM. Colchicine today. Joint Bone Spine. 2006, 1;73(6):672-8.
69. Ketrat S, Japrung D, Pongprayoon P. Exploring how structural and dynamic properties of bovine and canine serum albumins differ from human serum albumin. J Mol Graph Model. 2020, 98: 107601. Doi: 10.1016/j.jmgm.2020.107601.
70. Kosa T, Maruyama T, Otagiri M. Species differences of serum albumins: I. Drug binding sites. Pharm Res. 1997, 14(11): 1607-1612. Doi: 10.1023/a:1012138604016.
71. Amis TM, Renukuntla J, Bolla PK, Clark BA. Selection of cryoprotectant in lyophilization of progesterone-loaded stearic acid solid lipid nanoparticles. Pharmaceutics. 2020, 12(9): 892. Doi: 10.3390/pharmaceutics12090892.
72. Almalik A, Alradwan I, Kalam MA, Alshamsan A. Effect of cryoprotection on particle size stability and preservation of chitosan nanoparticles with and without hyaluronate or alginate coating. Saudi Pharm J. 2017, 25(6): 861–867. Doi: 10.1016/j.jsps.2016.12.008.
73. Lee MK, Kim MY, Kim S, Lee J. Cryoprotectants for freeze drying of drug nano-suspensions: effect of freezing rate. J Pharm Sci. 2009, 98(12): 4808–4817. Doi: 10.1002/jps.21786.
74. Corradini D, Strekalova EG, Stanley HE, Gallo P. Microscopic mechanism of protein cryopreservation in an aqueous solution with trehalose. Sci Rep. 2013, 3: 1218. Doi: 10.1038/srep01218.
75. Kratz F. Albumin as a drug carrier: design of prodrugs, drug conjugates and nanoparticles. J Controlled Release. 2008, 132(3): 171–183. Doi: 10.1016/j.jconrel.2008.05.010.
76. Verma D, Gulati N, Kaul S, Mukherjee S, Nagaich U. Protein based nanostructures for drug delivery. J Pharm. 2018: 9285854. Doi: 101155/2018/9285854.
77. Niknejad H, Mahmoudzadeh R. Comparison of different crosslinking methods for preparation of docetaxel-loaded albumin nanoparticles. Iran J Pharm Res. 2015, 14(2): 385-394.

SUPPLEMENTARIES

Molecular docking simulations

Ligand preparation

We used a molecular docking calculation to study ligand-albumin interactions. The ligands (two stereoisomers of CCI-001) structures were prepared using Ligprep from the Schrödinger suite (1). Conformations and tautomeric states were assigned to the ligands by following the ligand preparation protocol implemented in Schrödinger with default settings. LigPrep generates variants of the same ligand with different tautomeric, stereochemical, and ionization properties.

Albumin protein preparation

The crystallographic structure of the albumin is adopted from (PDB ID: 6WUW). Molecular Operating Environment (MOE) software package (2) is used to prepare the structure. The missing hydrogens for heavy atoms were added using the tLEAP module of AMBER 18 (3) with the AMBER17SB force field. The protonation states of all ionizable residues were determined at pH = 7 using the MOE program.

Binding pockets

The binding sites of the structures were identified through the MOE Site Finder program, which uses a geometric approach to calculate putative binding sites in a protein, starting from its three-dimensional structure. We used four binding pockets (Figure 1) for blind docking with (PLB>1). The PLB index can be used to predict the ligand-binding sites of uncharacterized protein structures and also to identify novel drug-binding sites of known drug targets (2).

Docking simulations Docking simulations were performed using the AutoDock Vina program (4) to predict the binding pose of the ligands under flexible ligand and rigid receptor conditions. The number of generated

ligand poses was set to 20 for every compound/protein structure pair. Docking simulations performed with a cubic box (size 30.0 Å) centered at the center of binding pockets and docking was run separately on the albumin structure. Every generated pose was energy-minimized using Amber14 (3). No constraints were applied in the docking studies. The pose with the best score was identified and shown in Figure 1. As it is possible to observe from the binding pose and location of CCI-001 to albumin, CCI-001 seems to bind near tryptophan, as the parent compound colchicine, but the location is slightly different.

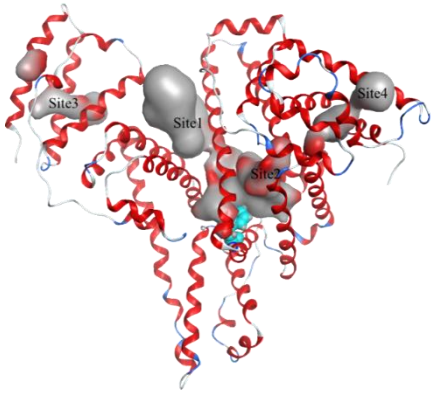

Figure 1S. Albumin protein binding sites (PLB>1). Tryptophan residue is shown in cyan color in ball representation.

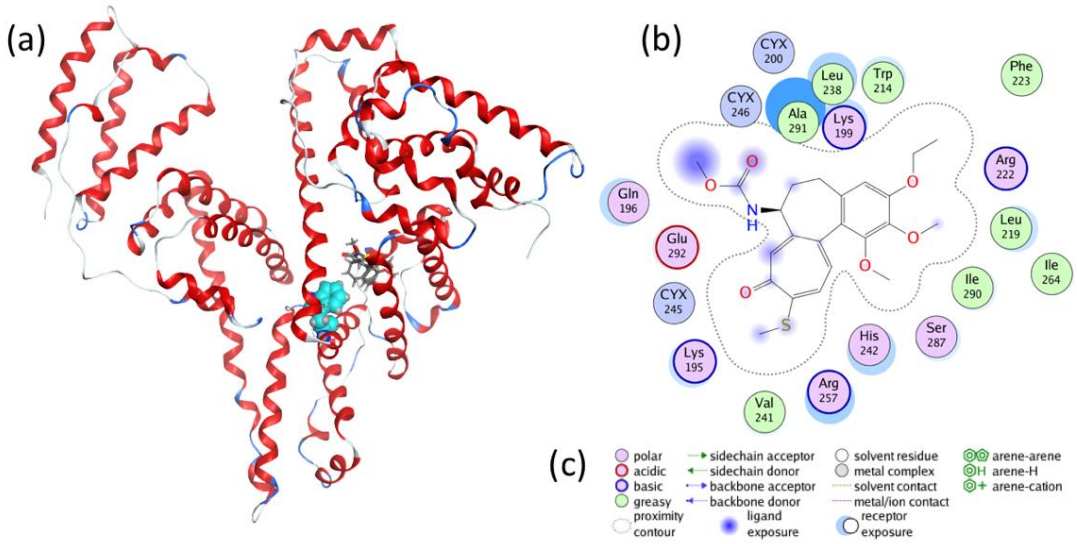

Figure 2S. Molecular docking studies of CCI-001 binding to albumin structure. (a) 3D and (b) 2D layout representation of CCI-001 in complex with albumin. Albumin is shown in cartoon representation (red). CCI-001 ligand is displayed with the stick and the atoms are colored as O (red), C (gray), N (blue), S (yellow), Cl (pink) and F(green). Tryptophan residue is shown in cyan color in ball representation. (c) Legend.

REFERENCES:

1. Schrödinger Schrödinger Release 2019–4: LigPrep. 2019. Available online: https://www.schrodinger.com/ligprep (accessed on 13 April 2020).
2. Molecular Operating Environment (MOE); Chemical Computing Group Inc: Montreal, QC, Canada, 2012.
3. Case, D.; Babin, V.; Berryman, J.; Betz, R.; Cai, Q.; Cerutti, D.; Cheatham, T., III; Darden, T.; Duke, R.; Gohlke, H.; et al. Amber 18; University of California: San Francisco, CA, USA, 2018.

4. Trott, O.; Olson, A.J. Software news and update AutoDock Vina: Improving the speed and accuracy of docking with a new scoring function, efficient optimization, and multithreading. *J. Comput. Chem.* 2010, *31*, 455–461.